Chemistry Europe
European Chemical Societies Publishing

Proton-Transfer Dynamics of Photoacidic Merocyanines in Aqueous Solution

Special Collection

Christoph Kaiser,[a] Thomas Halbritter,[b, c] Alexander Heckel,[c] and Josef Wachtveitl*[a]

Abstract: Photoacids attract increasing scientific attention, as they are valuable tools to spatiotemporally control proton-release reactions and pH values of solutions. We present the first time-resolved spectroscopic study of the excited state and proton-release dynamics of prominent merocyanine representatives. Femtosecond transient absorption measurements of a pyridine merocyanine with two distinct protonation sites revealed dissimilar proton-release mechanisms: one site acts as a photoacid generator as its pK_a value is modulated in the ground state after photoisomerization, while the other functions as an excited state photoacid which releases its proton within 1.1 ps. With a pK_a drop of 8.7 units to −5.5 upon excitation, the latter phenolic site is regarded a super-photoacid. The 6-nitro derivative exhibits only a phenolic site with similar, yet slightly less photoacidic characteristics and both compounds transfer their proton to methanol and ethanol. In contrast, for the related 6,8-dinitro compound an intramolecular proton transfer to the *ortho*-nitro group is suggested that is involved in a rapid relaxation into the ground state.

Introduction

Photoacids (PAs) turn into strong acids upon irradiation and thus enable light-stimulated proton dissociation. They steadily gain scientific attention, as they provide a convenient way to convert an optical input into a desired chemical response. If chosen properly, photoacids or photobases can in principle exert control over any proton- or pH-driven system with light as an outstanding external stimulus with unrivalled spatiotemporal precision. As a versatile trigger for proton-mediated processes, they can be exploited to regulate protein activity,[1,2] to design photoelectric circuits[3,4] and to advance functional materials.[5–7]

The generic term photoacid originally refers to compounds whose acidity is significantly enhanced when promoted to their electronically excited state (Scheme 1A). This entails an ultrafast proton dissociation or rather an excited state proton transfer (ESPT) to the solvent. First described as Förster cycle[8] this mechanism implies that the released proton is short-lived and reassociates thermally when the excited species relaxes back to its less acidic ground state.[9] An essential feature of a PA is its excited state dissociation constant pK_a*, which is correlated with the proton transfer rate. The pK_a* can be estimated by the Förster cycle model, while the proton transfer rates are typically determined by time-resolved spectroscopic techniques. In this context, various kinds of aryl-OH compounds are among the most extensively investigated photoacids. Examples like phenol or 1-naphthol (1N) exhibit lowered but still positive pK_a* values of 3[10] and 0.5,[11] respectively. In this acidity range 8-hydroxypyrene-1,3,6-trisulfonic acid (HPTS) also known as pyranine[12,13] is a prominent representative with a pK_a* = 1.3. The proton transfer process can take up to nanoseconds in aqueous solution for such photoacids with positive pK_a* values. Though, photoacids that adopt negative pK_a* values (< −1) were termed

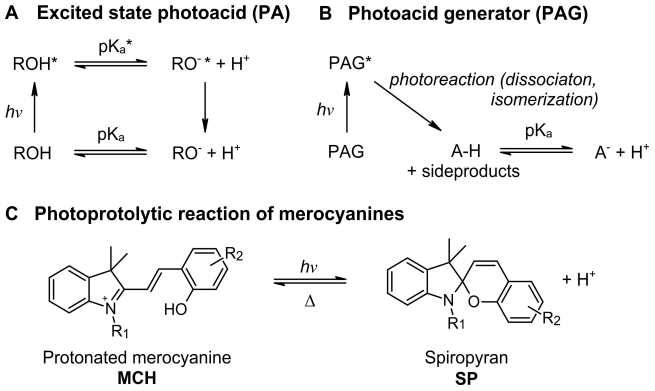

Scheme 1. Generalized proton-release reaction schemes **A**) of excited state photoacids (PA) following the Förster cycle, and **B**) of photoacid generators (PAG). **C**) Typical proton-release reaction of merocyanine-spiropyran photoswitches.

[a] C. Kaiser, Dr. J. Wachtveitl
Institute for Physical and Theoretical Chemistry
Goethe University Frankfurt/Main
Max-von-Laue-Str. 7, 60438 Frankfurt/Main (Germany)
E-mail: wveitl@theochem.uni-frankfurt.de

[b] Dr. T. Halbritter
Current address: Department of Chemistry, Science Institute
University of Iceland
Dunhaga 3, Reykjavik postcode is missing (Iceland)

[c] Dr. T. Halbritter, Dr. A. Heckel
Institute for Organic Chemistry and Chemical Biology
Goethe University Frankfurt/Main
Max-von-Laue-Str. 7, 60438 Frankfurt/Main (Germany)

Supporting information for this article is available on the WWW under https://doi.org/10.1002/chem.202100168

Special Collection This manuscript is part of an Indo-German special collection.

super-photoacids[14] and are even able to transfer their proton to alcohols within a few picoseconds. In several pioneering studies Tolbert and co-workers reported a series of 1N and 2-naphthol (2N) derivatives, where 5,8-dicyano-2-naphthol (DC2N) was found to be the strongest PA among them with a $pK_a^* = -4.5$.[11,14–16] Further related and even more photoacidic examples are hydroxyquinolinium compounds, which adopt pK_a^* values of ~ −7. Topp,[17] Ernsting[18] and Solntsev[19] reported the ESPT dynamics of *N*-methyl-6-hydroxyquinolinium (NM6HQ) and showed that proton dissociation occurs in a solvent-controlled manner within an excited state lifetime of 2–3 ps in aqueous solutions. More recently, Huppert *et al.* investigated several quinone cyanine dyes[20,21] (QCy), which are typically used as fluorophores for super-resolution microscopy. The highly conjugated dye QCy9 for example, exhibits a pK_a^* value as low as −8.5 and is thus the strongest photoacid studied so far.[22]

Following a mechanism different from ESPT, a proton-release can also occur as a result of a photoreaction cascade which makes the respective compound a photoacid generator (PAG, Scheme 1B).[23] After activation, PAGs allow for a high increase in proton concentration, but often irreversibly. They have been successfully utilized to initiate acid-catalyzed reactions[24] or cationic polymerization,[25] to create pH jumps[26] or photoacidic polymers.[27] They have also been applied as photoresists in microlithography.[28]

To this end, using photoswitches as photoacidic compounds can be very advantageous since they allow for a reversible operation of their protonation state, regardless of the nature of the photoacid itself. The reassociation of the proton is dictated by the isomerization of the photochromic compound and can be driven either thermally, photochemically or both.[29] Moreover, the (de-)protonation itself can essentially affect the properties of the respective photoswitch which can be applied to design multistimuli-responsive molecular logic systems.[30,31] Therefore, merocyanine-based photoacids, in particular benzo-indolino-pyrano-spiran (BIPS)[32,33] derivatives have been studied extensively for miscellaneous applications.[3,34–38]

Under acidic conditions, the ring-opened merocyanine form is protonated at its phenolate moiety (Scheme 1C). This proton is released upon photoisomerization towards the spiropyran structure and the compound thermally reverts to the protonated ring-opened form in the dark.[39–44] The pK_a value of this protonation site can be tuned by the choice of substituents on the respective phenyl ring (R_2 in Scheme 1C). For an unsubstituted ring a pK_a value of 7.8[39] is reported, while, for example, attachment of electron-withdrawing functionalities like an NO_2- or a CN-group in *para*-position drastically lowers the pK_a to 3.7 and 4.4, respectively.[35] Different proton-release pathways were postulated like an initial *cis/trans* photoisomerization of the protonated merocyanine followed by proton dissociation and ring-closure. Also the formation of a highly acidic spiropyran protonated on the indoline nitrogen has been discussed.[31,42] At very low pH values, an intramolecular transfer of the phenolic proton to the indoline nitrogen upon ring closure was suggested, where the latter protic site adopts a pK_a value below 1.6.[35] Yet, it has not been clarified whether the proton-release occurs from the excited merocyanine prior to the ring-closing sequence (excited state PA) or as consequence of the photoreaction due to the formation of an acidic photoproduct (PAG).

We previously investigated the photochromic properties of several pyridine derivatives of the parent BIPS compound, which we referred to as Py-BIPS.[45–47] Originally, the pyridine nitrogen of Py-BIPS-type compounds was methylated and therefore positively charged. More recently, we reported on an unmethylated Py-BIPS derivative, which shows refined photo- and acidochromic behaviour in aqueous solution.[48] The merocyanine isomer of this compound **1** and its protonated states are shown in Scheme 2A.

Due to the absence of the methyl group, merocyanine **1** exhibits a slightly acidic protonation site on its pyridine nitrogen ($pK_a^I = 6.8$), in addition to the phenolic site. Interestingly, the incorporation of the pyridine moiety lowers the pK_a^{II} value of the phenolic site to 3.2, which is even lower than the values of Nitro-BIPS derivatives. The pK_a of Nitro-BIPS **2** is 3.7[35] and that of Dinitro-BIPS **3** is 3.9[49] (Scheme 2B). Upon exposure to light, each of the shown protonated merocyanines is capable of photoinduced ring-closure which is accompanied by proton dissociation. In addition to protonated states, the existence of several *cis/trans*-isomers (the configurations of the three central double bonds are typically denoted by T for *trans* and C for *cis*) should be considered when investigating merocyanine compounds spectroscopically (Scheme 2C).[32] Eight isomers are possible in principle, but only those with a central T bond are stable ones. It is known that the two most stable isomers – mainly TTC and a minor fraction of TTT – exist in an equilibrated solution. The absorption band of TTT is shifted bathochromically with respect to the dominant TTC isomer. For Nitro-[50] as well as Dinitro-BIPS[51] derivatives distinguishable photoisomerization pathways were assigned for the two main isomers in

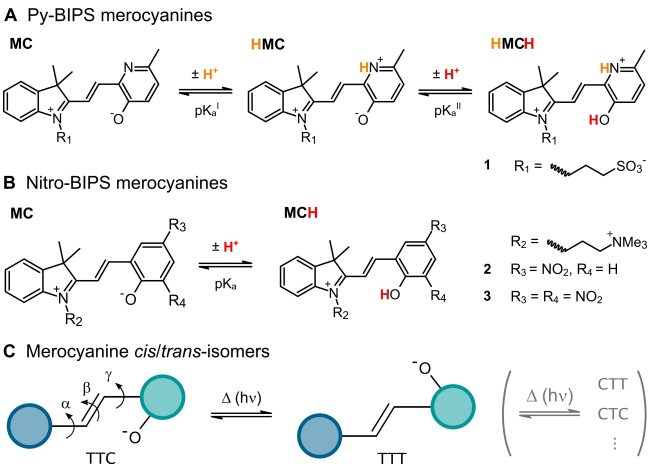

Scheme 2. Nomenclature of protonated species of the investigated **A**) Py-BIPS derivative **1** and **B**) Nitro-BIPS-type merocyanines **2** and **3. C**) Illustration of merocyanine *cis* (C)/*trans* (T) -isomers, referring to the configurations of the central double bond bridge. Rotation around the angles α, β and γ may occur thermally or photochemically. Among the eight possible isomers, those four with a T configuration at the middle bond are stable and the shown TTC and TTT (to a minor extent) are typically present in solution.

organic solvents, which might also be true for protonated merocyanines in general.

Here we present the first time-resolved investigation of the proton-release dynamics of photoacidic merocyanines by means of UV/vis-transient absorption (TA) spectroscopy in the fs-ns time window. We address the proton-release reactions of both protonation sites of compound **1** and of the phenolic sites of compounds **2** and **3** in order to shed light on the underlying mechanisms. The observed dynamics allow for a clear discrimination between photoacid generation and excited state photoacidity and provide clear evidence that the phenolic protonation site of the photoacidic merocyanines functions as a superphotoacid. Comparison with additional experiments in protic organic solvents give further insights into the ESPT dynamics of excited state PAs and the photoprotolytic cyle in general.

Results and Discussion

Photodynamics of MC and HMC of compound 1

The compounds **MC** and **HMC** (Scheme 2A) were investigated at pH 7.4 and 5.5, respectively, to ensure the maximal amount of the particular isomers. The photoinduced ring-closure reaction causes the pK_a^I value of the pyridine nitrogen to shift from 6.8 down to 4.8 for the spiropyran structure. Due to this outstanding side effect of photoswitching, we could realize a light-controlled steady-state pH value regulation of aqueous solution in a pH range roughly from 4.5 to 7. A pH drop of about 1.5 units was monitored upon exposure of an equilibrated **HMC** sample to visible light (520 nm) and the initial pH value was recovered within 5 minutes in the dark.[48] A comprehensive summary of the photophysical acidochromic properties of compound **1** is provided in the Supporting Information (see Figure S1). However, the fact that a significant persistent pH drop can be observed, implies that a thermal reassociation of the released proton is hindered after photoisomerization to the ring-closed structure. Thus, the observable pH drop apparently relies on the change of acidity of the peculiar *N*-protic site and the reprotonation is only feasible via ring opening. It remains unclear though, whether the proton is released as consequence of ring-closing or due to an increased excited state acidity of **HMC*** (excited states are indicated by asterisks).

The time-dependent spectral evolution during the first 1.5 ns of the ring-closing sequence of **MC** and **MCH** upon excitation with 520 nm at pH 7.4 and 5.5, respectively, is shown in Figure 1. The contour plots display the absorption difference relative to the ground state absorption. Hence, positive signals can be assigned to excited state absorption (ESA) or to the absorption of emerging intermediate species. Negative signals appear because of the ground state bleach (GSB) upon electronic excitation and due to stimulated emission (SE) induced by the probe pulse. In the transient map of **MC** (Figure 1A, left panel), a positive signal at 425 nm (ESA_1) and a more pronounced one around 505 nm (ESA_2) is observed. Both appear directly upon excitation and can thus be ascribed to the

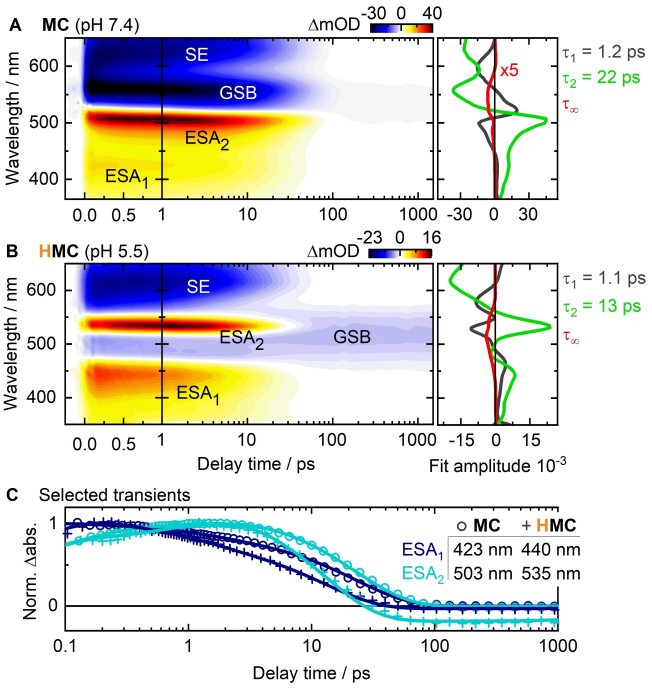

Figure 1. A) TA contour plot of **MC** of compound **1** at pH 7.4 (left panel) and corresponding DAS (right panel). **B)** TA contour plot of **HMC** of compound **1** at pH 5.5 (left panel) and corresponding DAS (right panel). **C)** Selected transients showing the time-dependent progression of the signals ESA_1 (blue) and ESA_2 (cyan) for **MC** (circles) and **HMC** (plus signs). Data points are represented by symbols and the fit from GLA by solid lines.

excited S1 state **MC***. Moreover, the negative SE signal around 620 nm resembles the steady-state emission of **MC** and the GSB is visible around 540 nm, where the ground state absorption band is centred (Figure S1). All of the excited state signals (both ESAs and SE) decay on a similar timescale and are almost vanished after 100 ps.

The kinetics observed in the TA spectra were analyzed by fitting the data sets globally with a sum of a given number of exponential lifetime components, which is referred to as global lifetime analysis (GLA).[52] From this procedure, decay-associated spectra (DAS) are obtained, which show the wavelength-dependent amplitudes of the determined lifetimes (Figure 1A and B, right panels). The reading of the DAS is as follows: a positive amplitude captures the decay of a positive absorption difference signal or a build-up of a negative signal. Inversely, a negative amplitude indicates a decay of a negative or an increase of a positive signal. Analysis of the TA spectrum of **MC** via GLA revealed that two main time constants are sufficient to describe the observed dynamics adequately. An additional infinite time constant τ_∞ reflects the residual signal at the end of the measurement after 1.5 ns. A schematic depiction of the assumed mechanism is given in Scheme 3A. The determined 1.2 ps lifetime (τ_1) models the solvent reorganization and vibrational relaxation within the S1 state **MC*** as the sigmoidal shape of its DAS captures a slight blue-shift of the ESA signals and a dynamic Stokes shift of the SE. However, the slower constant $\tau_2 = 22$ ps accounts for the decay of the signals

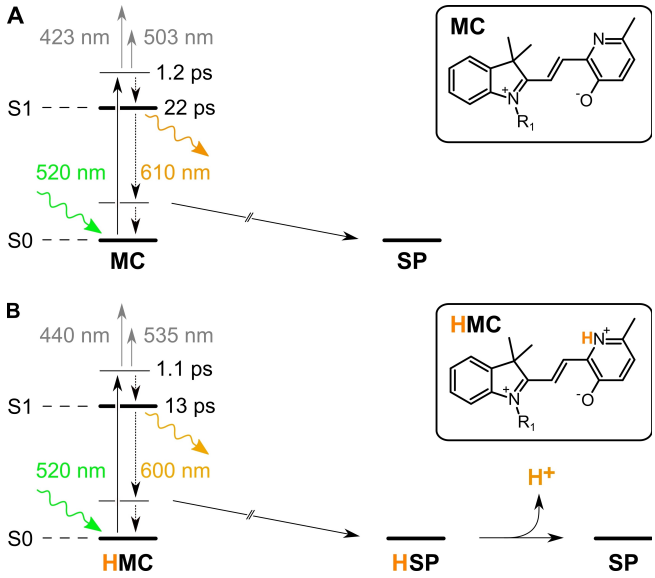

Scheme 3. Photoreaction pathway schemes of Py-BIPS **1. A)** Ring-closure dynamics of **MC** at pH 7.4. **B)** Ring-closure dynamics of **HMC** and subsequent proton-release from the **HSP** ground state at pH 5.5.

associated with the electronically excited state and is therefore ascribed to its lifetime. The large negative contribution of τ_2 around 560 nm indicates that the decay of **MC*** mostly recovers the initial **MC** ground state through SE but also non-radiatively. Last, the infinite time constant τ_∞ reveals that residual GSB is present at the end of the measured time frame due to the formation of the ring-closed photoisomer **SP**. Interestingly, there is no indication for the formation of a protonated state upon excitation of **MC**. Thus, the pyridine group plausibly does not acquire a proton from the solvent when excited as one could expect since related compounds like quinoline or acridine are known to be photobases.[53,54]

Just as the transient map of **MC**, the spectrum of **HMC** (Figure 1B, left panel) exhibits two separated ESA signals, although both are shifted to longer wavelengths by about 30 nm. Thus, the GSB appears in between the positive ESA signals. Similarly, the ESAs shift hypsochromically with time. Apart from the GSB, there is a pronounced negative SE signal around 610 nm. Data analysis indicates two main time constants reflecting an analogous spectral evolution as for **MC** (Figure 1B, right panel). First, the fast time constant $\tau_1 = 1.1$ ps models a rapid relaxation within the S1 state **HMC***, due to an initial motion away from the Franck-Condon region and to solvent reorganization. Then, the decay of the excited state is monitored by τ_2, which is significantly accelerated compared to **MC*** (13 ps vs. 22 ps). At the end of the measured time, again GSB is the only observed residual signal. The significant acceleration of the photodynamics of **HMC** compared to **MC** is also evident in view of the transient signal evolution depicted in Figure 1C. Similar dynamics for each of the signals are observed, where it takes approximately 80 ps for the **MC*** excited state signals to decay thoroughly and only about 40 ps for **MCH***. In both cases, the more pronounced ESA_2 seems to increase during the first ps, but this effect can be ascribed to the superposition of the respective ESA and the GSB.

The similarities in the **MC** and **HMC** photodynamics hint at analogous ring-closure pathways for both compounds. Furthermore, the observed dynamics is in agreement with the singlet pathway of the previously reported Py-BIPS[45] compound, where the decay of the excited state is further accelerated to 3.2 ps. These observations account for a distinct correlation between the substitution on the pyridine nitrogen and the excited state lifetime of the ring-open merocyanine. Starting from a mere lone pair on the nitrogen (**MC**) to a proton (**HMC**) to a methyl-group (Py-BIPS), the electron density on the N-atom decreases, which enhances the excited state decay. Although the formation of the photoproduct **HSP** could not be directly monitored here due to limitations of the probe light (broken arrows, Scheme 3), we suggest that ring-closure proceeds similarly to the parent Py-BIPS derivative. Hence, upon excitation of the thermodynamically favoured *trans*-merocyanine, ring-closure occurs via a series of *cis-trans* isomerizations from the vibrationally hot ground state of the ring-open isomer.[45,55] An indirect indication for these isomerizations is that the remaining GSB signal is slightly shifted with respect to the steady-state absorption band. The planar *trans*-merocyanine converts into a *cisoid* intermediate which already adopts a perpendicular structure and finally establishes the C–O bond.

In our previous study,[48] a fluorescence quantum yield of ~9% was determined for **MC** by integrating sphere measurements. Hence, non-radiative decay such as internal conversion or vibrational relaxation occurs with a ~91% probability. Starting from a vibrationally hot **MC** ground state, ring-closure is assumed to occur with a yield of ~5%, according to steady-state switching experiments. Compared to **MC**, the excited state decay of **HMC** is significantly faster and a lower fluorescence quantum yield of ~3.5% was found, which entails a probability of ~96.5% for non-radiative relaxation. Moreover, the quantum yield for photoproduct formation (**SPH**) is slightly higher at pH 5.5 (~7%) than at pH 7.4 (**SP**). This points to a favoured establishment of the ring-closed form when the pyridine nitrogen is protonated.

Concerning the proton-release of **HMC** it appears that the decay of the excited state is not accompanied by the emergence of an intermediate state. Hence, a dissociation of the proton in the excited state can be ruled out, as this would imply the formation of the excited deprotonated **MC***. **HMC** therefore does not release H^+ within the excited state but directly converts into the ring-closed structure **HSP** (Scheme 3B). This entails that **HMC** has to be considered as a reversible PAG rather than an excited state PA. The proton is released subsequently after formation of **HSP** and the observable pH jump therefore merely results from the altered pK_a value of the respective protic site.

Photo- and ESPT-dynamics of HMCH of compound 1

The TA spectrum of the doubly protonated **HMCH** in aqueous solution at pH 1 is shown in Figure 2A. Several signals are

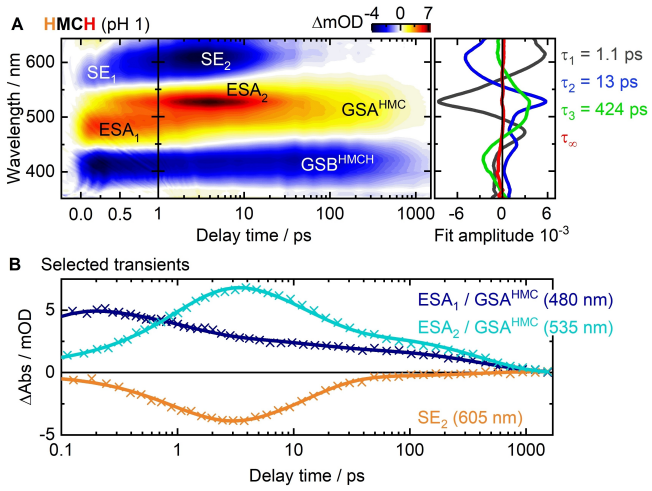

Figure 2. A) TA contour plot of **HMCH** of compound **1** at pH 1 (left panel) and corresponding DAS (right panel). **B)** Selected transients showing the time-dependent progression of the signals ESA_1 (blue), ESA_2 (cyan) and SE (orange). Data points are represented by symbols (crosses) and the fit from GLA by solid lines.

present directly upon excitation – the GSB at 420 nm and two ESA signals around 480 nm (ESA_1) and above 625 nm (not denoted). Moreover, an SE signal is detectable already at early times in between the ESA bands. Besides the GSB, the listed signals correspond to the excited **HMCH*** species. The positive amplitude of the time constant $\tau_1 = 1.1$ ps between 450 nm and 500 nm, where ESA_1 is located (Figure 2A, DAS), is indicative of an ultrafast decay of the initial excited species. The pronounced negative amplitude of τ_1 around 530 nm reveals that the decay of ESA_1 is accompanied by the emergence of a second positive signal (ESA_2) at 530 nm. The positive amplitude of τ_1 above 570 nm additionally captures the formation of the main SE_2 signal around 610 nm. Therefore, this time constant corresponds to a transition from **HMCH*** to a distinct new transient species. Comparison of the transients between 0.2 and 4 ps (Figure 2B) illustrates that the decay of ESA_1 and the increase of ESA_2 and SE_2 indeed occur with one rate. The spectral signature of the state, evolving with the constant τ_1 (ESA_2 and SE_2), coincides with that of the excited single protonated **HMC*** (ESA_2 and SE, see Figures 1B and S2) when the GSB is considered. The decay of ESA_2 and SE_2 is described by a similar time constant $\tau_2 = 13$ ps with a DAS that resembles the one found for **HMC*** which further confirms the assignment of the **HMC*** state. Hence, the release of the phenolic proton of **HMCH*** can be directly observed here and evidently occurs in the excited state. This process interestingly takes place on the same timescale as relaxation within the excited state in the cases of **MC** and **HMC**. Consequently, the proton is transferred to the solvent rather efficiently even before the **HMCH*** state is thoroughly relaxed on the S_1 potential energy surface. Competing deactivation channels for **HMCH*** are non-radiative decay and fluorescent emission. A fluorescence maximum at 470 nm was observed in the steady-state spectra and the red edge of this emission band that extends to roughly 600 nm is detected in the shape of SE_1.

After the proton transfer and the transition to **HMC***, the decay towards the ring-closed structure progresses analogously to the dynamics observed upon direct excitation of **HMC**. A simplified photoreaction and proton-release mechanism is provided in Scheme 4. The weaker ESA band of **HMC*** at 440 nm is not clearly visible in the contour plot (Figure 2A) due to the superposition with the GSB. Another small, positive signal below 370 nm can be noticed between 1 ps and 10 ps that also corresponds to **HMC***. Furthermore, the amplitudes of τ_1 and τ_2 indicate a rise and decay behaviour of the respective signal. Interestingly, the 13 ps lifetime exhibits no negative amplitude in the range of the GSB, which means that a recombination process of the proton from **HMC*** straight to the **HMCH** ground state is not indicated here.

After roughly 10–30 ps the sharp ESA_2 signal of **HMC*** superimposes with an emerging broad positive signal between 450 and 580 nm, which decays on a longer timescale but is almost vanished after 1.5 ns. The slow depletion of this broad signal can be observed in the spectral range where ESA_1 was located (Figure 2B). This broad absorption signal matches the time-integrated absorption spectrum of **HMC** and can thus be attributed to its ground state absorption (GSA). The positive amplitude of the time constant $\tau_3 = 424$ ps around 500 nm reflects the decay of the respective signal. Since the negative amplitude of τ_3 in the wavelength range of the GSB captures a repopulation of the **HMCH** ground state, we assign the respective time constant to the thermal reassociation of the proton. This reprotonation process completes the photoprotolytic Förster cycle roughly within the first nanosecond after excitation. At the end of the monitored time window the remaining bleach signal around 420 nm, described by the infinite time constant, reflects the conversion of some of the molecules into the spiro form.

Similar to **HMC**, a fluorescence quantum yield of ~3.5% was determined for **HMCH**.[48] Non-radiative relaxation of **HMCH*** certainly represents a considerable decay channel as the amplitude of τ_3 exhibits a ground state recovery contribution. However, the proton dissociation channel is suggested to be the predominant decay pathway, which is further supported by the fact that ESA_1 (**HMCH***) seems to thoroughly convert into ESA_2 (**HMC***) with mostly one lifetime. Assuming that radiative relaxation of **HMC*** again occurs with ~3.5% probability, non-

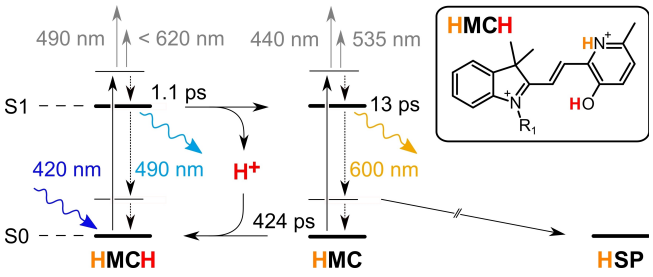

Scheme 4. Photoreaction pathway scheme of the excited state proton-release and ring-closure of **HMCH** of Py-BIPS **1** at pH 1.

radiative decay is again the major channel. Though, an overall quantum yield of **SPH** formation of ~10% was obtained by steady-state experiments, which is even higher than upon excitation of **HMC**. If this is due to relative excess energy provided by the high efficiency of the photoprotolytic decay channel towards **HMC*** remains speculative.

The pK_a* of the excited state can be estimated by applying the Förster cycle, which provides a simplified thermodynamic model for photoprotolytic processes. Equation (1) gives the correlation between the free energies ΔG of the proton dissociation processes in the ground and excited state and the transition energies of the acid AH and conjugate base A^-.[56,57]

$$E_{AH} - E_{A^-} = \Delta G - \Delta G^* = -RT(lnK_a - lnK_a^*) \quad (1)$$

To determine these energies, the transition energy differences between the vibrational ground states of S0 and S1 have to be estimated. Therefore, the most reasonable approach is to average the frequencies of the absorption and emission maxima of the acid (ν_{ROH}) and the conjugate base (ν_{RO^-}) as observed in steady-state experiments. Then the difference of the pK_a values of the ground and excited state is obtained by Equation (2).

$$pK_a - pK_a^* = N_A h(\nu_{ROH} - \nu_{RO^-})/2.3RT \quad (2)$$

Here, N_A is Avogadro's number, h Planck's constant and R the universal gas constant. With a ground state $pK_a = 3.2$ of **HMCH** this estimation results in a substantial pK_a drop of 8.7. Therefore, an excited state pK_a* of −5.5 is determined, which makes this merocyanine isomer one of the strongest super-photoacids reported, significantly more acidic than 1N or HPTS. Regarding its pK_a* value, **HMCH** is most comparable to the naphthol derivative DC2N[11] ($pK_a^* = -4.5$) or to the QCy derivatives like, for example, QCy7[20] ($pK_a^* = -5.7$). The ultrafast proton transfer within less than 1.1 ps and the striking pK_a drop indicate a pronounced enhancement of the acidity of **HMCH*** upon excitation. The photoacidity basically depends on the charge distribution in the excited state and the stabilization of the negative charge of the deprotonated form. In case of merocyanines, the negative charge is in general highly delocalized due to the expanded conjugation of the molecule and can be displaced from the phenolate oxygen to the indolinium nitrogen. Because of that, the neutral quinoid mesomeric resonance structure of the core chromophore strongly contributes to the stabilization. Moreover, a pronounced redistribution of π-electrons is suggested to take place upon excitation of aromatic photoacids, which facilitates the proton-release process.[58]

Following theory, the ESPT mechanistically occurs in two consecutive steps.[58–62] Upon electronic excitation, the proton is transferred from an aromatic photoacid ROH* to an adjacent water or solvent molecule with an intrinsic rate. This creates a solvent stabilized contact ion pair, with a distinct contact radius [Eq. (3)]:

$$ROH^* \rightleftharpoons [RO^{-*} \cdots H^+] \quad (3)$$

With further increase of the distance between the ions the proton becomes thoroughly solvated or rather is transferred to larger water clusters. This step is apparently dictated by the diffusion of the proton away from the anion into the bulk solvent and is therefore strongly affected by solvent properties and electrostatic interactions. Therefore, the timescale of this diffusive step is typically much longer than that of the initial proton abstraction on contact [Eq. (4)]:

$$[RO^{-*} \cdots H^+] \rightleftharpoons RO^{-*} + H^+ \quad (4)$$

A mathematical treatment engages the Debye-Smoluchowski equation (DSE) that takes the random thermal motion into account as well as the Coulomb potential between the ions.[63] The back reaction is referred to as diffusion-assisted geminate recombination, which is substantially influenced by the electric field of the conjugate base anion.

In the case of **HMCH***, the initial step of the photoprotolytic reaction occurs within 1.1 ps in water. This translates into an overall proton transfer rate $k_{pt} = 9.1 \times 10^{11}\ s^{-1}$. The formation of ESA_2 (Figure 2A) is ascribed to the contact ion pair, as this is assumed to adopt identical spectral properties as the deprotonated RO^{-}*. There are no clear indications for a major contribution of the back reaction since ESA_1 seems to convert entirely into ESA_2. Though, the existence of the equilibrium can be verified since a pH dependent fluorescence emission of **HMCH*** is observed in the steady state. Interestingly, the initial proton transfer occurs on a similar timescale as solvent relaxation dynamics. The Debye relaxation time of water around a solute molecule is found to be approximately 1 ps[17] and the proton hopping time from one water molecule to another is roughly 1.5 ps.[62] Hence, the proton transfer from **HMCH*** to a water molecule proceeds even faster than the proton transfer in between water molecules via the Grotthuss mechanism. The subsequent diffusion is supposed to occur similarly fast in aqueous solution, although this is influenced by the electric field of the conjugate base anion. Apart from the negative phenolate charge, the deprotonated merocyanine **HMC*** exhibits two positively charged nitrogen atoms. In addition, the compound bears a flexible negatively charged sulfonic acid residue that could exert enhancing effects on geminate recombination.

To gain more insights into the ESPT dynamics and to verify whether **HMCH** is capable of transferring its proton to poorer proton acceptors like organic solvents, we conducted additional TA experiments in the protic solvents methanol (MeOH) and ethanol (EtOH) and the aprotic solvent acetonitrile (MeCN) at pH 1. Although, both protic solvents are capable of H-bonding, they are significantly less polar. While water exhibits a dielectric constant ε of 78, those of MeOH and EtOH are 33 and 24, respectively. The dielectric constant of MeCN is 37 and is therefore comparable to MeOH. The obtained transient maps in MeOH and EtOH show almost the same spectral signature as

observed in water, although the signals are slightly shifted hypsochromically (see Figures S3 and S4).

The decay of the initially formed ESA_1 and SE_1 of **HMCH*** is accompanied by the emergence of ESA_2 and SE_2 within the first ps. The latter two signals are again assigned to the excited state of the conjugate base **HMC***. An ultrafast ESPT of the phenolic proton therefore evidently occurs also in protic organic solvents.

Apart from that, the decay of ESA_1 is slowed down with decreasing proton acceptor capabilities of the solvents. As the formation of ESA_2 and SE_2 is also delayed it can be noted that the ESPT is decelerated in the order from water to MeOH to EtOH. Furthermore, the relative intensities of the ESA_2 signals in the protic solvents compared to ESA_1 are smaller than in water, which hints at a less efficient process. Accordingly, the SE_2 signal is significantly less pronounced, too. In the kinetic analysis of the data sets, a similar number of lifetime components as in water was determined (Figure 3A). The respective lifetimes are of similar orders of magnitude and their amplitudes mostly resemble analogous contributions. Yet, the measurement in aprotic MeCN revealed no emergence of the excited conjugate base signals (see Figure 3B). Only the signals originating from **HMCH*** are visible, which decay substantially slower than in water and the protic solvents. Therefore, the lifetime of the excited state **HMCH*** is elongated. However, a proton transfer to MeCN can be ruled out, although it is the organic solvent with the highest polarity among the investigated ones.

In the GLA of the MeOH and EtOH measurements, time constants of 1.7 ps and 1.9 ps, respectively, were determined to describe the proton transfer processes (Figure 3A). Despite the before mentioned hypsochromic shift of the signals, the amplitudes of these time constants are in excellent agreement with the 1.1 ps constant found in aqueous solution. Hence, the ESPT is significantly slower than in water but roughly similarly fast in MeOH and EtOH. The time constants found for the subsequent decay of **HMC*** are also slower in MeOH (16 ps) and EtOH (24 ps) than the 13 ps constant in water. The respective time constants exhibit positive contributions in the range of ESA_1 around 490 nm, which are absent in the DAS of the lifetime determined in water. This might indicate that a pronounced fraction of ESA_1 decays on a 10–30 ps timescale and the actual lifetime of the **HMCH*** state is prolonged in both protic solvents. The biphasic decay of ESA_1 furthermore shows that a slowed down decay channel competes with proton dissociation. A similar timescale of the ESA decay was also observed in the MeCN measurement. A 10 ps lifetime was determined for the main decay channel of **HCMH*** and an additional 33 ps lifetime was found. The latter captures a decay of a positive band around 500 nm as well as the formation of a positive absorption signal above 550 nm and a repopulation of the ground state. The respective lifetime might thus account for the decay of a distinguishable merocyanine isomer, which is excited simultaneously or which is formed in the excited state through isomerization. Although the photodynamics are suggested to be dominated by the TTC isomer (Scheme 2C), the observed signals may be superimposed with those of the TTT isomer. The lifetime components τ_2 found in MeOH and EtOH therefore supposedly represent mixed lifetimes that comprise additional decay dynamics of **HMCH***. In any case, the biphasic decay of ESA_1 modelled by τ_1 and τ_2 implicates competing deactivation pathways that lower the efficiency of proton dissociation.

The lifetimes τ_2 furthermore exhibit negative amplitudes below 475 nm and thus model a recovery of the **HMCH** ground state, in contrast to the corresponding lifetime found in water. Hence, in organic solvents a proton recombination quenching of **HMC*** seems to occur, which could be assisted by the negatively charged sulfonate residue. In aqueous solution this process might occur too, but significantly less pronounced. As in water, the formation of the broad GSA of **HMC** (450–550 nm) can be observed in both TA maps of the protic solvents (Figures S3 and S4) after the ESA_2 decay. The relative intensity of this long-term feature decreases significantly in the order from water to MeOH to EtOH, which provides another evidence that the efficiency of the photoprotolytic decay of **HMCH*** also decreases in that order. In contrast to the measurement in water, the depletion of this signal is not completed at the end of the accessible time window after 1.5 ns. The **HMC** ground state is therefore still present in both protic solvents.

However, to fit the data sets adequately by GLA, a third lifetime component had to be engaged, that captures a partial decay of the **HMC** ground state towards **HMCH**. This lifetime τ_3 exhibits a much smaller relative amplitude than the corresponding 424 ps lifetime determined for reprotonation in water and it is accelerated to 320 ps in MeOH and 254 ps in EtOH. The amplitudes of τ_3 in the protic solvents exhibit a minor

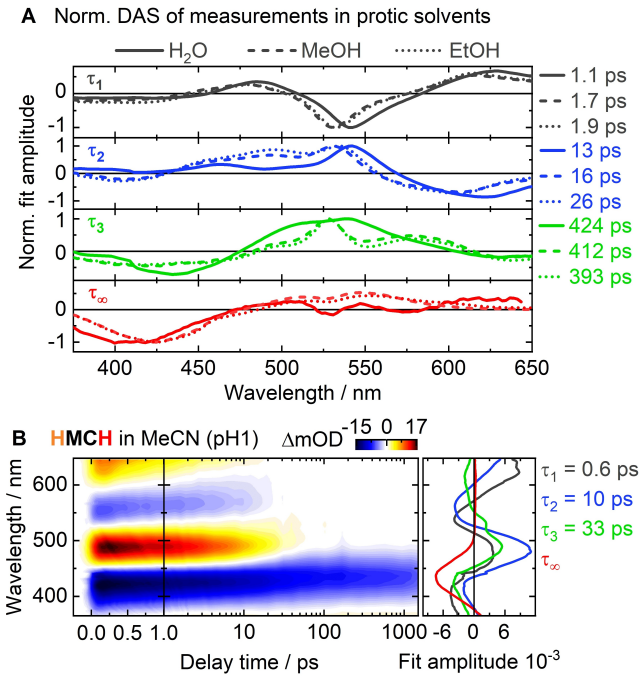

Figure 3. A) Comparison of the determined DAS of the TA measurements of **HMCH** of compound **1** in H_2O (solid lines), MeOH (dashed lines) and EtOH (dotted lines). **B)** TA contour plot of **HMCH** of compound **1** at pH 1 in MeCN (left panel) and corresponding DAS (right panel).

contribution to the decay of ESA_2 and a slower decay component of the SE_2 signal. This hints at a non-exponential long-term decay of the excited conjugate base. An accelerated reprotonation process seems plausible, if it is due to geminate recombination, as the solvation of the free proton is less favoured in both organic solvents than in water. Here, again the sulfonate residue supposedly plays an important role in arranging the nearby solvation shell of the photoacid. An exclusively diffusion-driven reprotonation process, following the DSE model, should be much slower in the protic solvents, since the diffusion coefficients of the proton are significantly smaller than in water. Thus, the electrostatic potential of the negatively charged and flexible residue supposedly affects the diffusion of the proton and assists to the recombination. Moreover, the amplitudes of τ_3 reveal a decay contribution in the red flank of the overall GSA signal (575 nm) in the protic solvents. The blue region of the signal around 550 nm is still present after 1.5 ns, which is captured by the infinite lifetimes. This might again be ascribed to the presence of two merocyanine conformers, where one undergoes the reprotonation process faster than the other. Upon excitation, the main TTC-merocyanine converts into a ground state *cisoid* structure which either undergoes ring-closure or reverts back to the initial *trans*-configuration and adopts a red-shifted absorption band.[64] Hence, the decay of the red flank of the GSA signal might account for the *cisoid*-form which favours the reprotonation process due to its particular geometry.

As additional model-free data evaluation method, lifetime distribution analyses (LDA) were performed on each data set. The obtained lifetime density maps (LDM) for the three solvents are depicted and further compared in the Supporting Information (see Figure S6). The LDMs represent the time-dependent distribution of lifetime components, obtained from fitting the data sets with a high number of lifetimes (>100). In contrast to the GLA, this analysis is thus not biased by a kinetic scheme and a given set of contributing lifetimes. It therefore provides a better representation of the actual timescales of the assigned processes. The reading of the LDM contour plots, however, is similar as for the DAS. A positive amplitude indicates the decay of a positive signal or the increase of a negative one and vice versa.

Proton-transfer dynamics of Nitro-BIPS derivative 2

TA experiments were conducted with the protonated form of the extensively applied 6-nitro-BIPS derivative **2** (Scheme 2B). In acidified aqueous solution, the spiropyran-merocyanine equilibrium is shifted to the energetically favoured protonated merocyanine **MCH** and thermal conversion to the ring-closed isomer is not observed anymore. The photophysical properties in neutral aqueous solution as well as the ultrafast dynamics are reported elsewhere.[47] A brief description of the steady-state behaviour in the neutral and acidic pH range may be found in the Supporting Information, together with the absorption and emission spectra of the **MC** and **MCH** states (Figure S7). The ground state pK_a value of compounds **2** is 3.7.[35] Thus, the TA measurements were carried out at pH 1 to accumulate the pure protonated state.

The transient map of Nitro-BIPS **2**, shown in Figure 4A, reveals initial signals that can clearly be assigned to the excited S1 state **MCH***. Around 560 nm the negative signal SE_1 appears directly upon excitation, as well as a prominent positive signal (ESA_1) and a minor ESA band below 425 nm (not denoted). The latter overlaps with the GSB around 410 nm, which also emerges instantaneously upon excitation. The minor ESA below 425 nm vanishes after around 1 ps just as the signal SE_1, which is accompanied by the formation of the even more pronounced SE_2 around 610 nm. This spectral evolution already hints at the formation of the excited conjugate base, as SE_2 fits the steady-state emission thereof.[47] The prominent ESA_1 prevails until roughly 100 ps but evolves into a broad positive signal between 450 nm and almost 600 nm. Here, the interpretation is not unequivocal at first, due to the superposition of multiple signals. Yet, in comparison with the reported TA data of the deprotonated **MC**[47] the assignment becomes clear. The deprotonated form exhibits an SE signal between 575 nm and 650 nm and one pronounced ESA signal around 450 nm, both lasting until approximately 100 ps. The similarity of this spectral signature and the observed signal of **MCH** (ESA_1) indicate that both the acid and the conjugate base exhibit ESA signals around 450 nm, impeding a precise discrimination in the spectrum in Figure 4A.

The ESA_1 transient at 485 nm (Figure 4B) reveals an initial ultrafast decrease within the first 700 fs, followed by a slower depletion of the signal. According to the DAS (Figure 4A, right panel), a sub-ps lifetime was found ($\tau_1 = 0.4$ ps), which is ascribed to an initial cooling process within the excited S1 state **MCH***, as it models a slight shift of the corresponding signals. The lifetime $\tau_2 = 2.1$ ps captures the decay of the minor ESA below 425 nm as well as the decay of SE_1 and the subsequent formation of SE_2. In the wavelength range around ESA_1 the

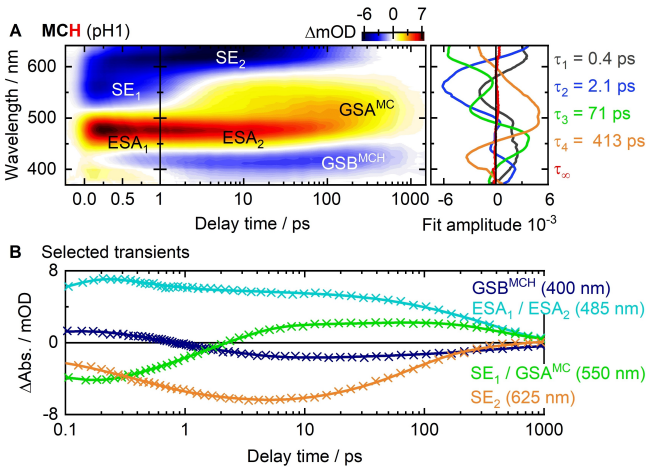

Figure 4. A) TA contour plot of **MCH** of compound **2** at pH 1 (left panel) and corresponding DAS (right panel). **B)** Selected transients showing the time-dependent progression of the signals GSB (blue), ESA_1 and ESA_2 (cyan), SE_1 and GSA^{MC} (green) and SE_2 (orange). Data points are represented by symbols (crosses) and the fit from GLA by solid lines.

amplitude of this lifetime is almost zero. However, we assign τ_2 to the proton-release process, as illustrated in Scheme 5, primarily because it accounts for the transition from SE_1 (**MCH***) to SE_2 (**MC***). Yet, as the signal SE_2 already emerges within the first 0.5 ps, the proton transfer is supposed to start during the vibrational relaxation process. If the transition from SE_1 to SE_2 is just fitted with one lifetime component, a lifetime of 1.6 ps is determined, which therefore reflects the mean value of the proton transfer lifetime component. This estimation results in a proton transfer rate $k_{pt} = 6.3 \times 10^{11}\ s^{-1}$. However, compared to compound **1** the quantum yield of the ESPT process is suggested to be similarly high, since the SE_1 signal is entirely converted into SE_2. The minor ESA below 400 nm shows similar decay dynamics as SE_1 which also speaks against a large contribution of additional competing dynamics.

The subsequent decay of ESA_2 and SE_2, that correspond to **MC***, is modelled by time component $\tau_3 = 71$ ps (positive amplitude around 450 nm and negative amplitude above 575 nm). Therefore, it can be attributed to the lifetime of the respective state and a lifetime in the same order of magnitude and with a similar DAS was found upon direct excitation of **MC**.[47] The negative amplitude of τ_3 between 490 nm and 575 nm accounts for the emergence of another positive signal (ESA_2) whose decay is modelled by the broad positive amplitude of $\tau_4 = 413$ ps in this range. This absorption band is related to the **MC** ground state. As τ_4 features a negative amplitude below 450 nm it also captures a repopulation of the **MCH** ground state. Hence, τ_4 describes the reprotonation process, which completes the photoprotolytic cycle on the same timescale as observed for compound **1**. Interestingly, the reprotonation in the ground state proceeds with almost similar lifetimes for both merocyanine derivatives **1** and **2**, as the pK_a values of the acid ground states are rather similar. This is indicative of a diffusion-driven recombination with the solvated proton. Apparently, the alkyl residue attached to the indoline nitrogen does not affect the reprotonation in aqueous solution, as the two compounds exhibit differently charged functional groups.

Based on the steady-state absorbance and fluorescence data (Figure S7), again the excited state pK_a* of **MCH*** could be obtained. With a $pK_a = 3.7$, the Förster cycle estimation yields a pK_a drop of 7.9 units and a $pK_a^* = -4.2$. This is only slightly less acidic than the Py-BIPS PA **1** discussed before and Nitro-BIPS **2** has to be considered a super-photoacid as well. The attachment of the NO_2-group exerts a smaller electron-withdrawing effect on the phenolic oxygen than the incorporated nitrogen of Py-BIPS and the charge displacement upon optical excitation is less pronounced.

The photoprotolytic reaction of **MCH** of compound **2** was also measured in the solvents MeOH, EtOH and MeCN. The TA spectra of **MCH** in MeOH (Figure 5A) and EtOH (Figure S8) show very similar features and monitor clear indications for a proton transfer to the solvent. In the protic solvents, the signal SE_1 of **MCH*** is longer lived and SE_2 of **MC*** is significantly less pronounced which is indicative of the proton transfer. A time constant of $\tau_1 = 2.4$ ps was found for the proton transfer in both protic solvents as it models the transition from SE_1 to SE_2 (Figure 5B). It also captures a partial decay of the superimposed ESA_1/ESA_2 signal and the decay of the minor ESA below 400 nm, that also corresponds to **MCH***. The following decay of the ESA_1/ESA_2 feature seems significantly accelerated compared to water and it evolves into the broad absorption signal of the **MC** ground state, which is also less pronounced. The decay of the ESA signal is captured by two more lifetime components. While the main decay is modelled by a 17 ps (18 ps) in MeOH (EtOH), a considerable contribution decays with a significantly longer lifetime of 290 ps (298 ps). The corresponding amplitudes are in good agreement for both protic solvents. The amplitude of the 71 ps lifetime found in water for the particular ESA decay is rather resembled by the slower lifetime components than the faster ones, regarding the minimum in the near-UV and the region above 500 nm (Figure 5B). However, both the fast and the slow components show contributions to the formation of the broad GSA signal and the decay of SE_2 but at different

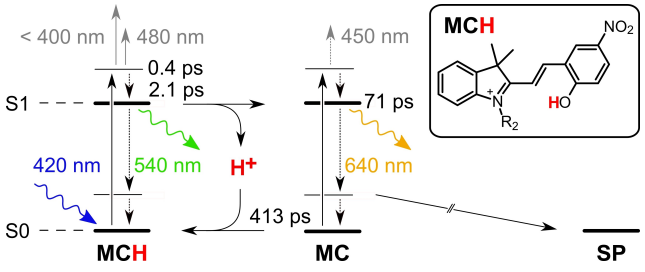

Scheme 5. Photoreaction pathway scheme of the excited state proton-release and ring-closure of **MCH** of Nitro-BIPS **2** at pH 1.

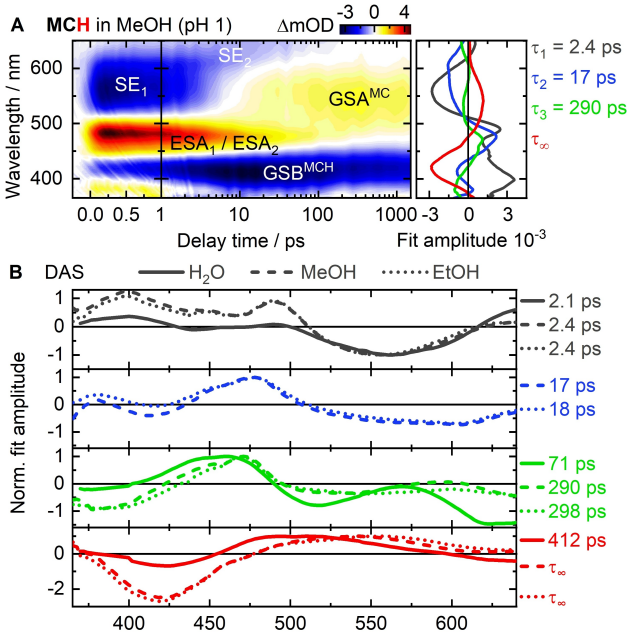

Figure 5. A) TA contour plot of **MCH** of compound **2** in MeOH (left panel) and corresponding DAS (right panel). **B)** Comparison of the DAS determined through GLA for the three solvents H_2O (solid lines), MeOH (dashed lines) and EtOH (dotted lines). The lifetime components are sorted by highest agreement.

wavelength ranges. Therefore, the respective two lifetimes are supposedly attributed to different *cis-trans* merocyanine isomers that undergo the discriminable relaxation pathways.

Especially concerning Nitro-BIPS derivatives, different isomerization sequences have been reported for particular conformers in various solvents.[64] Ruetzel et al. found that in MeCN the TTC isomer converts into the TTT in the excited state unidirectionally within 200 fs and both forms decay on different timescales afterwards.[50] An SE signal around 625 nm was assigned to the TTC isomer while that of the TTT form is shifted bathochromically by 30 nm. Therefore, we ascribe the lifetime τ_2, which models the decay of the blue region of SE_2 to the TTC conformer. The longer lifetime τ_3 with a smaller relative amplitude then presumably corresponds to TTT which represents the isomer, typically existing to a smaller extent. After 1.5 ns, there is still a pronounced positive signal around 550 nm, which is in good accordance with the reported ground state absorption of the TTC isomer. This, as well as a prominent residual fraction of the **MCH** bleach signal, is reflected by the infinite time constants determined in both protic solvents (Figure 5B). Their amplitudes are in good agreement with the 412 ps lifetime component determined in water. Hence, the ground state reprotonation seems to be essentially slower than in water and also than in the case of compound **1**. Here again, this might be influenced by the alkyl residue attached to the indoline nitrogen. Compound **2** bears a positively charged functionality, which is supposed to exert a repulsive effect on the released proton and therefore hinders a diffusion-assisted recombination.

The essentially reduced efficiency of the photoprotolytic decay of **MCH*** in MeOH and EtOH hints at the existence of other major reaction channels than in water. Besides fluorescence relaxation also non-radiative decay into the ground state may occur. Internal conversion is reported to be a considerable pathway for Nitro-BIPS derivatives, also because of the enhancing effect of the nitro group.[65] Moreover, the contribution of triplet states to the photodynamics of Nitro-BIPS is well-known,[64] although no distinct indications were found here. Non-radiative decay is suggested to yield a vibrationally hot ground state which undergoes further cooling. This cooling process causes the observed bathochromic shift of the GSB signal after 100 ps (Figure 5A). However, the remaining bleach after 1.5 ns resembles the ground state absorption spectrum quite well.

In the measurement in MeCN (Figure S11) similar **MCH**-associated signals were detected as in the protic solvents, like an ESA around 480 nm and SE around 570 nm and both decay on a similar timescale within 10–20 ps. As no emergence of signals that could be assigned to the excited conjugate base was observed, a proton transfer can be ruled out. Though, a positive absorption signal from 500 nm to 625 nm appearing after 20 ps is detected, which accounts for a deprotonated merocyanine ground state absorption. This could either arise from small amounts of water within the measured sample that the proton is transferred to or to residual amounts of non-protonated merocyanine that undergoes the isomerization observed by Ruetzel *et al.* The GLA revealed a vibrational relaxation of **MCH*** with a lifetime of 1.1 ps. Interestingly, a lifetime of 7.5 ps was determined here for the **MCH*** decay of the main isomer (TTC), which is essentially faster than the lifetimes reported for the non-protonated Nitro-BIPS analogue.

Proton-transfer dynamics of Dinitro-BIPS derivative 3

For the Dinitro-BIPS derivatives **3** (Scheme 2B), the ring-opened **MC** isomer is even more stabilized than for the nitro compound **2**. In aqueous solution, compound **3** is therefore more prone to hydrolysis. Though, the photoswitching properties are quite comparable to compound **2** just as the excited state dynamics of the unprotonated **MC** isomer.[47] With a pK_a value of 3.9,[49] the protonated **MCH** state is formed upon acidification, which is thermally stable at pH 1 and shows fluorescence emission around 495 nm. A brief summary of the behaviour in aqueous solution may be found in the Supporting Information, with corresponding absorption and emission spectra of the **MC** and **MCH** states (Figure S7). Based on these spectra, again the pK_a* value can be estimated for compound **3** by use of the Förster cycle approximation. The resulting pK_a drop of 8.3 units is even more pronounced than that of the nitro compound **2**. Ultimately, a pK_a* value of −4.2 is determined for **MCH** of compound **3** is, which makes it a super-photoacid.

The TA measurement of **MCH** of the Dinitro-BIPS derivative **3** at pH 1 revealed an essentially different behaviour than the before presented PAs **1** and **2**. The TA spectrum (Figure 6A) displays two ESA signals centred around 470 nm and 600 nm, where the latter is more intense by a factor of roughly 2.5. Those positive signals as well as the GSB at 400 nm decay almost completely within 1 ps. This implies, that the compound mainly relaxes back into its ground state non-radiatively upon optical excitation. After roughly 30 ps, all observed signals virtually decay to zero, as the transients in Figure 6B illustrate.

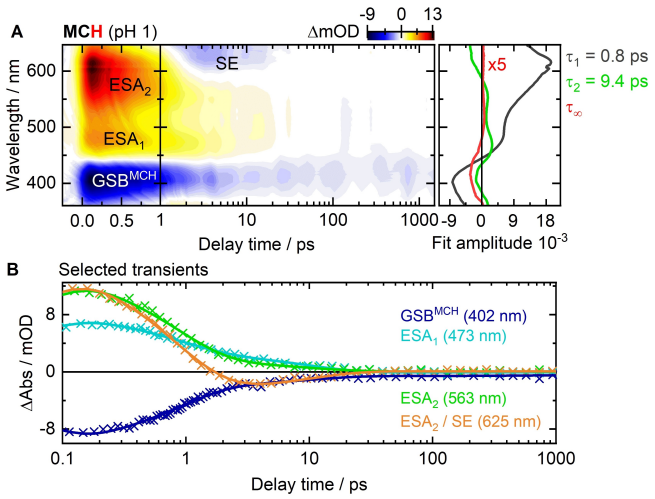

Figure 6. A) TA contour plot of **MCH** of compound **3** in MeOH at pH 1 (left panel) and corresponding DAS (right panel). **B)** Selected transients showing the time-dependent progression of the signals GSB^{MCH} (blue), ESA_1 (cyan), ESA_2 (green) and ESA_2 and SE_2 (orange).

However, a small portion of the GSB signal remains until the end of the measurement. The ESA features decay with a 0.8 ps time constant and leave two small blue-shifted positive signals around 460 nm and 550 nm behind. After approximately 1.5 ps, a small negative SE signal is noticeable above 600 nm which decays with the same time constant (9.4 ps) as the respective minor positive signals. These signals and the corresponding lifetime are assigned to the conjugate base **MC***, as they are in good agreement with the reported spectral signature, although the weak ESA around 550 nm could not be observed upon direct excitation of **MC** at pH 7.4 due to the superimposed prominent bleach signal.[47] The reported lifetime of the excited **MC***state is 8.7 ps, which further confirms this assignment. The amplitude of the lifetime determined here exhibits a small contribution to the ground state recovery, which indicates a proton-recombination induced quenching process. The 0.8 ps thus models the transition from **MCH*** to **MC*** and is associated with the proton transfer rate $k_{pt} = 1.3 \times 10^{12}\ s^{-1}$. After the depletion of the **MC*** signals, there is almost no residual signal observable. Only the infinite time constant reveals a weak positive residual signal around 520 nm that corresponds to the conjugate base ground state. An additional lifetime component for the reprotonation process could not be determined.

The peculiar photodynamics of compound **3**, compared to compounds **1** and **2**, apparently arise from the additional nitro group in *ortho*-position to the acidic hydroxyl group of **MCH**. With a partially negative charge on both oxygen atoms of the nitro group, it may stabilize the hydroxyl proton already in the ground state and react as proton acceptor upon excitation. The photodynamics of *o*-nitro benzyl (*o*NB) compounds is known to involve an initial excited state intramolecular proton transfer (ESIPT) but typically from an alkyl α-H-atom to the nitro group.[66–68] This results in the formation of the tautomeric *aci*-nitro form (=NO_2H) through parallel singlet and triplet pathways, which is frequently exploited for the subsequent removal of photolabile protecting groups.[69,70] Regarding compound **3**, an ultrafast ESIPT to the 8-nitro group might therefore be an considerable reaction channel, although no distinguishable spectroscopic characteristics of this species are observed here. However, since **MCH*** of compound **3** mostly decays into its ground state, the *o*NB group might facilitate the proton-induced recombination quenching of the **MC*** state via transient *aci*-nitro formation.

Similar to Nitro-BIPS derivatives, the presence of the TTC and TTT isomer has been reported for the non-protonated dinitro-analogues.[71] The TTC form also represents the most stable one with a main absorption band around 560 nm, while the TTT absorbance is shifted to longer wavelengths. An interconversion between the two conformers is not supposed to be a significant reaction pathway. In this study, we found no indications for discriminable isomers and the photodynamics are suggested to be dominated by the TTC isomer.

Correlation between free-energy and ESPT rates

The determined photoacidic characteristics of the three investigated compounds are summarized in Table 1. It is noticeable that the ground state pK_a values are in a similar range. This entails, that the electron distribution at the phenolate moiety is influenced in a comparable way. The attachment of the electron withdrawing nitro substituents and the incorporation of the pyridine ring evidently lower the pK_a value to a similar extent and the estimated pK_a changes upon optical excitation are quite similar, too. Compound **1** yet exhibits the lowest pK_a* value and thus the most pronounced charge displacement in the excited state.

The relationship of the extracted proton transfer rate constants and the estimated pK_a* values can be further rationalized by a semi-empirical correlation, which is based on the Marcus theory for electron transfer processes[72] yet modified for proton transfer. This gives a major role to the alignment of solvent molecules in the vicinity of the dissociating proton.[73,74] Accordingly, the proton transfer process is described by a solvent coordinate along an pre-existing hydrogen bond. The rate k_{pt} is then expressed as a function of the intrinsic solvent-dependent activation free-energy change $\Delta G^{\#}$ of the reaction [Eq. (5)]:

$$k_{pt} = k^* \cdot exp\left(-\frac{\Delta G^{\#}}{RT}\right) \tag{5}$$

Here, $(k^*)^{-1}$ represents the frequency factor of the transfer reaction, R is the gas constant, and T the absolute temperature. The free energy change $\Delta G^{\#}$ is estimated by the Marcus bond-energy-bond-order (BEBO) model [Eq. (6)]:[75]

$$\Delta G_0 = \frac{\Delta G_0}{2} + \Delta G^{\#} + \frac{\Delta G_0{}^{\#}}{ln2}\, ln\left(cosh\left[\frac{\Delta G_0 ln2}{2\Delta G_0{}^{\#}}\right]\right) \tag{6}$$

The free-energy of the charge-exchange with the solvent is given by $\Delta G_0{}^{\#}$ if the total free-energy in the PT process ΔG_0 is zero [Eq. (7)]:

$$\Delta G_0 = RT\ ln10\ \Delta pK_a \tag{7}$$

The correlation of the determined rate constants k_{pt} of the compounds **1**–**3** and the pK_a* values, estimated by the Förster

Table 1. Photoacidic properties of the excited state PAs of the Py-BIPS derivative **1**, the nitro-BIPS compound **2** and the dinitro-BIPS compound **3** in water.

	1 (HMCH)	**2** (MCH)	**3** (MCH)
pK_a	3.2	3.7	3.9
ΔpK_a	−8.7	−7.9	−8.3
pK_a*[a]	−5.5	−4.2	−4.4
τ (ROH*) [ps]	1.1	2.1	0.8
k_{pt}[b] [s^{-1}]	$\sim 9.1 \times 10^{11}$	$\sim 6.3 \times 10^{11}$	$\sim 1.3 \times 10^{12}$

[a] Excited state pK_a* values, determined by the Förster cycle approach, [b] ESPT rate coefficients obtained from GLA.

cycle, is depicted in Figure 7. The solid line represents the Marcus BEBO model fit including the reported PT rates of a variety of comparable photoacids with pK_a* values around zero or below. Several phenol,[10] 1N,[75,76] 2N[16] and hydroxy quinoline (HQ)[73,77] derivatives are shown, as well as the beforementioned QCy[20,78] compounds.

For PT reactions to bulk water the pK_a* is corrected for the purely electrostatic contribution $pK_{a,el} = R_D/2.3a$.[79] A charge of −1 for the conjugate base is assumed for the Debye radius R_D and the contact radius a was set to be 6.5 Å.[80] In the fitting procedure, k* was treated as a free parameter and a value of roughly 5×10^{12} s^{-1} was obtained which represents the proton transfer rate for an activationless process. Similarly, an intrinsic free-energy barrier of $\Delta G_0^{\#} = 3.5$ kcal mol^{-1} was found, which is close to reported values.[81,82] Consequently, the determined rates k_{pt} of the herein investigated merocyanine PAs are in well agreement with the applied literature-based structure-reactivity correlation, including super-photoacids with pK_a* values lower than −4. The compounds **1**–**3** are significantly more acidic than most naphthol derivatives. They are situated in the highly exothermic regime of the correlation curve together with the structurally related QCy7, S-QCy7 and TS-QCy compounds. The photoacidity of the studied merocyanine PAs as well as the QCy dyes is additionally enhanced due to the high degree of charge delocalization through the molecular structure and the formation of the quinoid form. The strongest reported photoacid QCy9 even exceeds the boundaries of the correlation model with its remarkable proton transfer rate of ~10^{13}.[22,78] This is close to the stretching mode frequency of an OH-bond which is on the order of almost ~10^{14} s^{-1}.

The findings further corroborate the estimated pK_a* values, that were derived from equilibrium conditions. These values can therefore hardly describe dynamic characteristics of ESPT processes. For instance, the compounds **1**–**3** exhibit several charged functional groups, such as the flexible ionic alkyl residues at the indoline nitrogen, that may contribute to a pre-organization of the solvent shell which facilitates the ESPT processes. The establishment of an aligned solvent network stabilized by polar or hydrogen bonding moieties affects proton dissociation differently than bulk water arrangements and also extends the lifetime such water wires.[83] Especially the anionic sulfonate group of **1** might exert a significant effect in this fashion. For S-QCy7 and TS-QCy, bearing similar functional groups, a sulfonate-assisted proton dissociation is suggested, too.[20] Yet, because of the different PT rates found in the protic solvents MeOH and EtOH a direct proton transfer to the sulfonate group can be excluded here.

Regarding the measurements in alcoholic solvents, it has to be noted that minor amounts of water were present in the sample solutions, because of acidification with aqueous HCl. Again, the observed varying proton transfer rates compared to water indicate that it's not a pure water cluster that is arranged around the acidic proton and that it is transferred to, although the solvent distribution might not be homogeneous.[79] Moreover, the measurements in MeOH and EtOH revealed an increased contribution of alternative decay channels of the excited PA that lower the efficiency of proton dissociation. For the Py-BIPS derivative **1**, ESPT rates of 5.9×10^{11} s^{-1} and 5.3×10^{11} s^{-1} were estimated in MeOH and EtOH, respectively. For Nitro-BIPS **2**, the contribution of competing pathways such as internal conversion is even more pronounced and similar ESPT rates of roughly 4.2×10^{11} s^{-1} were found in both protic solvents.

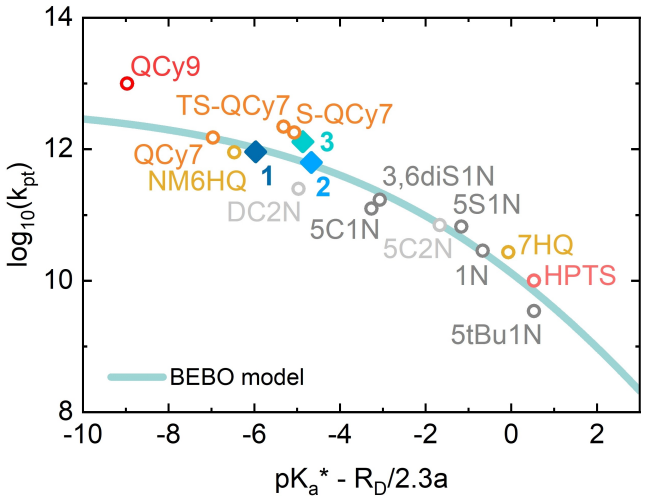

Figure 7. Free-energy correlation of determined rates k_{pt} of compounds **1**,**2** and **3** (filled diamonds) compared with comparable reported photoacids (empty circles). The solid line represents the Marcus bond-energy-bond-order (BEBO) model according to Equations 5–7.

Conclusion

Our results show that the phenolic protonation sites of the Py- as well as the Nitro-BIPS merocyanine photoacids investigated herein represent outstanding excited state PAs. They are capable of transferring their phenolic proton to water within a few ps upon optical excitation. Except for the dinitro derivative **3**, ESPT is highly efficient and the preferred deactivation pathway in aqueous solution. Compounds **1** and **2** are even capable of ESPT to protic organic solvents, although this is less efficient and slightly slowed down compared to water. Regarding compound **3**, an ESIPT to the *ortho*-located nitro group seems plausible that results in the formation of a transient *aci*-nitro form. Internal conversion and proton-induced quenching of the excited conjugate base are suggested be the major deactivation channels.

The proton-release mechanism itself has not yet been monitored directly on an ultrafast time scale but distinguishable pathways have been suggested, based on observations made in different steady-state experiments. Our findings imply that the release of the phenolic proton is the first step in the photodynamics upon excitation of merocyanine PAs. Hence, the involvement of the aforementioned protonated spiropyran species in the ring-closure reaction can be ruled out, as the proton is released prior to ring closing. This might furthermore not only be true for the presented photoacidic Py- and Nitro-BIPS derivatives but also for protonated merocyanine deriva-

tives in general. The TA measurements of the ultrafast ESPT reactions of compound **1** and **2** enabled the assignment of the entire photoprotolytic cycle, including the reprotonation in the ground state. As similar reprotonation lifetime components were determined for both compounds in water, the respective process is supposed to be solvent- and thus diffusion-controlled. The differently charged residues attached to the indoline nitrogen do not cause differences in the reprotonation dynamics. In contrast, this step seems to be influenced in the protic solvents. The negative charge of the sulfonate group of compound **1** is supposed to accelerate the reprotonation process partially with decreasing solvent polarity. On the contrary, the positive charge of the trimethylammonium group of compound **2** slows down the reprotonation in the protic solvents.

In addition, we could show that the N-protic site of compound **1** exhibits a fundamentally different reactivity. The proton is not released due to an enhanced excited state acidity, but subsequently upon isomerization to the spiropyran structure because of the ground state pK_a change. Hence, the respective protic site has to be considered a PAG rather than an excited state PA, although it also functions as a reversible photoacid. Yet, knowledge of the timescale and the dynamics of the proton-release is essential in view of potential applications of PAs. Especially when applied as a trigger for time-resolved studies of proton-mediated processes the proton transfer dynamics must be taken into account as well as limitations caused by diffusion.

The integration of the pyridine ring into the merocyanine structure of Py-BIPS derivatives has fascinating effects on the photochemistry and provides a valuable motif for future molecular design. Not only that this position allows for straightforward attachment of diverse substituents, but the photodynamics is understood quite well. Following a singlet pathway just as the original BIPS compound, the decay of the excited state is accelerated drastically starting from the unsubstituted pyridine nitrogen (MC) through the protonated (HMC) to the methylated Py-BIPS form.[45] Besides the retained ultrafast singlet pathway, the photophysical steady-state properties are affected severely by the respective substituents and can thus be tuned. Essential differences are for example found when comparing the behaviour of compound **1** at pH 7.4 with the methylated Py-BIPS compound. The lack of the methyl group of compound **1** results in a pronounced stabilization of the ring-opened merocyanine, which allows for an operation of the photoswitch as a negatively photochromic one using visible light only.

Experimental Section

Sample preparation. The synthesis of compound **1** was performed following the published procedure via aldol condensation of the alkylated indoline and the corresponding pyridine salicyle aldehyde.[48] The Nitro-BIPS compounds **2** and **3** were synthesized using the respective nitro-salicyl aldehydes.[47] The spectroscopic investigation was carried out in phosphate buffered saline (PBS buffer) except for the measurements in organic solvents. The pH values were adjusted with concentrated aqueous HCl. The absorption spectra of the particular photoisomers were recorded with a Specord S600 spectrophotometer (Analytik Jena AG, Jena, Germany) in 10 mm × 10 mm UV-grade quartz glass cuvettes (Starna GmbH, Pfungstadt, Germany). The emission spectra were measured with a JASCO FP 8500 spectrofluorometer (JASCO Germany GmbH, Groß-Umstadt, Germany) using 4 mm × 10 mm UV-grade quartz glass cuvettes (Starna GmbH). All spectra were offset corrected and the fluorescence spectra were additionally corrected for reabsorption effects as well as for the detector sensitivity of the spectrometer.

Femtosecond TA spectroscopy. The TA data were acquired with self-assembled UV/vis-pump/vis-probe setups, either supplied by a 1 kHz Ti:Sapphire amplifier (CPA, Clark-MXR, Michigan, USA) with a pulse duration of approximately 150 fs and a central wavelength of 775 nm or a Ti:Sapphire amplifier (Spitfire Ace, Newport Spectra-Physics GmbH, Darmstadt, Germany) with a pulse duration of 120 fs and a fundamental wavelength of 800 nm. The excitation pulses in the vis-range (520 nm) were generated with a non-collinear optical amplifier (NOPA) by guiding a supercontinuum pulse into a beta-barium borate crystal (β-BaB_2O_4, BBO) together with a second harmonic pulse at 388 nm. UV-pulses for excitation (420 nm) were generated by subsequent sum frequency generation (SFG) of the NOPA output and the fundamental in another BBO crystal. The white light continuum for probing (~350 nm–650 nm) was created by guiding the fundamental of the laser system through a 2 mm CaF_2 window. The samples for the time-resolved experiments were prepared in 1 mm UV-grade quartz glass cuvettes (Starna GmbH) and the concentrations were adjusted to an optical density of approximately 0.6. During the pump/probe experiments, the samples were illuminated with light emitting diodes (LED, ThorLabs Inc., Newton, New Jersey, USA) to accumulate the photoisomer of interest. In order to prevent a reexcitation of already excited molecules, the sample cuvettes were moved in an y-z-plane perpendicular to the excitation pulses. To eliminate anisotropy effects, the relative polarizations of the pump and probe pulses were adjusted to the magic angle (54.7°).

The obtained transient maps were processed and corrected for the group-velocity dispersion and the coherent artefact. The latter is fitted by a Gaussian function or its first and second derivative and subtracted from the data set. The TA spectra were then subjected to multiexponential fitting via global lifetime analysis (GLA) by using the kinetic fitting software OPTIMUS.[52] From this, lifetime components and their corresponding decay associated spectra (DAS) could be extracted. Additionally, a lifetime distribution analysis (LDA) was performed as a complementary and model-free approach (see Supporting Information).

Acknowledgements

We thank the Deutsche Forschungsgemeinschaft (DFG) for funding through, SFB 902 „Molecular Principles of RNA-based Regulation“, GRK 1986 “CLiC – Complex Light Control” and grant number WA 1850/4-2. Open access funding enabled and organized by Projekt DEAL.

Conflict of Interest

The authors declare no conflict of interest.

Keywords: cyanines · photoacid · proton transfer · spiro compounds · ultrafast spectroscopy

[1] S. Kohse, A. Neubauer, A. Pazidis, S. Lochbrunner, U. Kragl, *J. Am. Chem. Soc.* **2013**, *135*, 9407–9411.
[2] É. Lörinczi, M. Verhoefen, J. Wachtveitl, A. C. Woerner, C. Glaubitz, M. Engelhard, E. Bamberg, T. Friedrich, *J. Mol. Biol.* **2009**, *393*, 320–341.
[3] X. Xie, G. A. Crespo, G. Mistlberger, E. Bakker, *Nat. Chem.* **2014**, *6*, 202–207.
[4] S. Haghighat, S. Ostresh, J. M. Dawlaty, *J. Phys. Chem. B* **2016**, *120*, 1002–1007.
[5] W. White, D. Christopher, D. M. Fabian, W. White, C. D. Sanborn, D. M. Fabian, S. Ardo, *Joule* **2018**, *2*, 1–16.
[6] X. Su, S. Voskian, R. P. Hughes, I. Aprahamian, *Angew. Chem. Int. Ed.* **2013**, *52*, 10734–10739; *Angew. Chem.* **2013**, *125*, 10934–10939.
[7] X. Pan, H. Li, K. T. Nguyen, G. Gru, Y. Zhao, *J. Phys. Chem. B* **2012**, *116*, 4175–4181.
[8] T. Förster, *Naturwissenschaften* **1949**, *36*, 186–187.
[9] J. F. Ireland, P. A. H. Wyatt, *Adv. Phys. Org. Chem.* **1976**, *12*, 131–221.
[10] S. Kaneko, S. Yotoriyama, H. Koda, S. Tobita, *J. Phys. Chem. A* **2009**, *113*, 3021–3028.
[11] I. Carmeli, D. Huppert, L. M. Tolbert, J. E. Haubrich, *Chem. Phys. Lett.* **1996**, *4*, 109–114.
[12] O. F. Mohammed, J. Dreyer, B.-Z. Magnes, E. Pines, E. T. J. Nibbering, *ChemPhysChem* **2005**, *84125*, 625–636.
[13] R. Simkovitch, D. Huppert, *J. Phys. Chem. A* **2015**, *119*, 1973–1982.
[14] D. Huppert, L. M. Tolbert, S. Linares-Samaniego, *J. Phys. Chem. A* **1997**, *5639*, 4602–4605.
[15] L. M. Tolbert, K. M. Solntsev, *Acc. Chem. Res.* **2002**, *35*, 19–27.
[16] L. M. Tolbert, J. E. Haubrich, *J. Am. Chem. Soc.* **1990**, *112*, 8163–8165.
[17] T. G. Kim, M. R. Topp, *J. Phys. Chem. A* **2004**, *108*, 10060–10065.
[18] J. L. Pérez-Lustres, F. Rodriguez-Prieto, M. Mosquera, T. A. Senyushkina, N. P. Ernsting, S. A. Kovalenko, *J. Am. Chem. Soc.* **2007**, *129*, 5408f5418.
[19] E. A. Gould, A. V. Popov, L. M. Tolbert, I. Presiado, Y. Erez, D. Huppert, K. M. Solntsev, *Phys. Chem. Chem. Phys.* **2012**, *14*, 8964–8973.
[20] I. Presiado, N. Karton-lifshin, Y. Erez, R. Gepshtein, D. Shabat, D. Huppert, *J. Phys. Chem.* **2012**, *116*, 7353–7363.
[21] N. Karton-Lifshin, I. Presiado, Y. Erez, R. Gepshtein, D. Shabat, D. Huppert, *J. Phys. Chem. A* **2012**, *116*, 85–92.
[22] R. Simkovitch, S. Shomer, R. Gepshtein, M. E. Roth, D. Shabat, D. Huppert, *J. Photochem. Photobiol. A* **2014**, *277*, 90–101.
[23] J. V. Crivello, *J. Photopolym. Sci. Technol.* **2009**, *22*, 575–582.
[24] B. K. Keitz, R. H. Grubbs, *J. Am. Chem. Soc.* **2009**, *131*, 2038–2039.
[25] M. Shirai, I. Tsunooka, *Prog. Polym. Sci.* **1996**, *21*, 1–45.
[26] Z. Shi, P. Peng, D. Strohecker, Y. Liao, *J. Am. Chem. Soc.* **2011**, *133*, 14699–14703.
[27] N. Abeyrathna, Y. Liao, *J. Photochem. Photobiol. A* **2017**, *332*, 196–199.
[28] M. G. Ivan, J. C. Scaiano, in *Photochem. Photophysics Polym. Mater.* (Ed.: N.S. Allen), John Wiley& Sons, Inc., **2010**, pp. 479–507.
[29] Y. Liao, *Acc. Chem. Res.* **2017**, *50*, 1956–1964.
[30] J. Gurke, S. Budzák, B. M. Schmidt, D. Jacquemin, S. Hecht, *Angew. Chem. Int. Ed.* **2018**, *57*, 4797–4801; *Angew. Chem.* **2018**, *130*, 4888–4893.
[31] L. Kortekaas, J. Chen, D. Jacquemin, W. R. Browne, *J. Phys. Chem. B* **2018**, *122*, 6423–6430.
[32] N. P. Ernsting, T. Arthen-Engeland, *J. Phys. Chem.* **1991**, *95*, 5502–5509.
[33] M. Rini, A. K. Holm, E. T. J. Nibbering, H. Fidder, *J. Am. Chem. Soc.* **2003**, *125*, 3028–3034.
[34] S. Silvi, A. Arduini, A. Pochini, A. Secchi, M. Tomasulo, F. M. Raymo, M. Baroncini, A. Credi, *J. Am. Chem. Soc.* **2007**, *129*, 13378–13379.
[35] M. Hammarson, J. R. Nilsson, S. Li, T. Beke-Somfai, J. Andréasson, *J. Phys. Chem. B* **2013**, *117*, 13561–13571.
[36] P. K. Kundu, D. Samanta, R. Leizrowice, B. Margulis, H. Zhao, M. Börner, T. Udayabhaskararao, D. Manna, R. Klajn, *Nat. Chem.* **2015**, *7*, 646–652.
[37] P. Remón, S. M. Li, M. Grøtli, U. Pischel, J. Andréasson, *Chem. Commun.* **2016**, *52*, 4659–4662.
[38] S. Giordani, M. A. Cejas, F. M. Raymo, *Tetrahedron* **2004**, *60*, 10973–10981.
[39] Z. Shi, P. Peng, D. Strohecker, Y. Liao, *J. Am. Chem. Soc.* **2011**, *133*, 14699–14703.
[40] L. A. Tatum, J. T. Foy, I. Aprahamian, *J. Am. Chem. Soc.* **2014**, *136*, 17438–17441.
[41] N. Abeyrathna, Y. Liao, *J. Am. Chem. Soc.* **2015**, *137*, 11282–11284.
[42] S. Kusumoto, T. Nakagawa, Y. Yokoyama, *Adv. Opt. Mater.* **2016**, *4*, 1350–1353.
[43] H. Chen, Y. Liao, *J. Photochem. Photobiol. A* **2015**, *300*, 22–26.
[44] V. K. Johns, Z. Wang, X. Li, Y. Liao, *J. Phys. Chem. A* **2013**, *117*, 13101–13104.
[45] J. Kohl-Landgraf, M. Braun, C. Özçoban, D. P. N. Gonçalves, A. Heckel, J. Wachtveitl, *J. Am. Chem. Soc.* **2012**, *134*, 14070–14077.
[46] C. Özçoban, T. Halbritter, S. Steinwand, L.-M. Herzig, J. Kohl-Landgraf, N. Askari, F. Groher, B. Fürtig, C. Richter, H. Schwalbe, B. Suess, J. Wachtveitl, A. Heckel, *Org. Lett.* **2015**, *17*, 1517–1520.
[47] C. Kaiser, T. Halbritter, A. Heckel, J. Wachtveitl, *ChemistrySelect* **2017**, *2*, 4111–4123.
[48] T. Halbritter, C. Kaiser, J. Wachtveitl, A. Heckel, *J. Org. Chem.* **2017**, *82*, 8040–8047.
[49] J. Zhou, Y. Li, Y. Tang, F. Zhao, X. Song, E. Li, *J. Photochem. Photobiol. A* **1995**, *90*, 117–123.
[50] S. Ruetzel, M. Diekmann, P. Nuernberger, C. Walter, B. Engels, T. Brixner, *J. Chem. Phys.* **2014**, *140*, 1–10.
[51] J. Buback, P. Nuernberger, M. Kullmann, F. Langhojer, R. Schmidt, F. Würthner, T. Brixner, *J. Phys. Chem. A* **2011**, *115*, 3924–3935.
[52] C. Slavov, H. Hartmann, J. Wachtveitl, *Anal. Chem.* **2015**, *87*, 2328–2336.
[53] E. W. Driscoll, J. R. Hunt, J. M. Dawlaty, *J. Phys. Chem. A* **2017**, *121*, 7099–7107.
[54] E. T. Ryan, T. Xiang, K. P. Johnston, M. A. Fox, *J. Phys. Chem. A* **1997**, *101*, 1827–1835.
[55] Y. Sheng, J. Leszczynski, A. A. Garcia, R. Rosario, D. Gust, J. Springer, *J. Phys. Chem. B* **2004**, *108*, 16233–16243.
[56] B. Marciniak, H. Kozubek, S. Paszyc, *J. Chem. Educ.* **1992**, *69*, 247–249.
[57] Z. R. Grabowski, W. Rubaszewska, *J. Lumin.* **1981**, *24*, 559–562.
[58] A. Weller, *Z. Elektrochem.* **1952**, *56*, 662.
[59] M. Eigen, *Angew. Chem. Int. Ed.* **1964**, *3*, 1–19; *Angew. Chem.* **1963**, *75*, 489–508.
[60] N. Agmon, *J. Phys. Chem. A* **2005**, *109*, 13–35.
[61] B. Cohen, D. Huppert, N. Agmon, *J. Phys. Chem. A* **2001**, *105*, 7165–7173.
[62] N. Agmon, *Chem. Phys. Lett.* **1995**, *50*, 456–462.
[63] P. Debye, *J. Appl. Phys.* **1975**, *46*, 265–272.
[64] A. K. Chibisov, H. Görner, *J. Phys. Chem. A* **1997**, *101*, 4305–4312.
[65] H. Fidder, M. Rini, E. T. J. Nibbering, *J. Am. Chem. Soc.* **2004**, *126*, 3789–3794.
[66] H. Takahashi, Y. Watanabe, M. Sakai, M. Tachikawa, *Laser Chem.* **1999**, *19*, 357–362.
[67] J. Kohl-Landgraf, F. Buhr, D. Lefrancois, J. M. Mewes, H. Schwalbe, A. Dreuw, J. Wachtveitl, *J. Am. Chem. Soc.* **2014**, *136*, 3430–3438.
[68] P. Naumov, *J. Mol. Struct.* **2006**, *783*, 1–8.
[69] A. P. Pelliccioli, J. Wirz, *Photochem. Photobiol. Sci.* **2002**, *1*, 441–458.
[70] C. G. Bochet, *J. Chem. Soc. Perkin Trans. 1* **2002**, *2*, 125–142.
[71] M. Kullmann, S. Ruetzel, J. Buback, P. Nuernberger, T. Brixner, *J. Am. Chem. Soc.* **2011**, *133*, 13074–13080.
[72] A. O. Cohen, R. A. Marcus, *J. Phys. Chem.* **1968**, *72*, 4249–4256.
[73] M. Ekimova, F. Hoffmann, G. Bekçiog˘lu-Neff, A. Rafferty, O. Kornilov, E. T. J. Nibbering, D. Sebastiani, *J. Am. Chem. Soc.* **2019**, *141*, 14581–14592.
[74] O. F. Mohammed, D. Pines, E. Pines, E. T. J. Nibbering, *Chem. Phys.* **2007**, *341*, 240–257.
[75] M. Prémont-Schwarz, T. Barak, D. Pines, E. T. J. Nibbering, E. Pines, *J. Phys. Chem. B* **2013**, *117*, 4594–4603.
[76] E. Pines, D. Pines, T. Barak, B.–Z. Magnes, L. M. Tolbert, J. E. Haubrich,„ *Ber. Bunsenges. Phys. Chem.* **1998**, *102*, 511–517.
[77] E. Bardez, *Isr. J. Chem.* **1999**, *39*, 319–332.
[78] R. Simkovitch, K. Akulov, S. Shomer, M. E. Roth, D. Shabat, T. Schwartz, D. Huppert, *J. Phys. Chem. A* **2014**, *118*, 4425–4443.
[79] E. Pines, G. R. Fleming, *J. Phys. Chem.* **1991**, *95*, 10448–10457.
[80] E. Pines, D. Huppert, N. Agmon, *J. Chem. Phys.* **1988**, *88*, 5620–5630.
[81] K. Adamczyk, M. Prémont-Schwarz, D. Pines, E. Pines, E. T. J. Nibbering, *Science* **2009**, *326*, 1690–16994.
[82] N. Agmon, *Int. J. Chem. Kinet.* **1981**, *13*, 333–365.
[83] G. Bekçioğlu, C. Allolio, D. Sebastiani, *J. Phys. Chem. B* **2015**, *119*, 4053–4060.

Manuscript received: January 15, 2021
Accepted manuscript online: April 30, 2021
Version of record online: June 1, 2021

